Anal. Chem. **2010,** *82,* 3537–3546

Coupling Surface-Enhanced Resonance Raman Scattering and Electronic Tongue as Characterization Tools to Investigate Biological Membrane Mimetic Systems

Pedro H. B. Aoki,[†] Priscila Alessio,[†,‡] Antonio Riul, Jr.,[§] J. A. De Saja Saez,[‡] and Carlos J. L. Constantino*[,†]

Faculdade de Ciências e Tecnologia, Unesp Univ Estadual Paulista, Presidente Prudente/SP, 19060-900, Brazil, Faculty of Science, University of Valladolid, Valladolid 47011, Spain, and Universidade Federal de São Carlos, campus Sorocaba/SP, 18043-970, Brazil

The surface-enhanced Raman scattering (SERS) effect and sensor and biosensor analyses are widely applied to investigate drug−biomolecule interactions or to detect trace amount of analytes. In this work, surface-enhanced resonance Raman scattering (SERRS) and an electronic tongue system using impedance spectroscopy were brought together, combining sensitivity and structural level information. Taking advantage of the use of layer-by-layer (LbL) films of phospholipids as biological membrane mimetic systems, cardiolipin (CLP) and dipalmitoyl phosphatidyl glycerol (DPPG) were applied as transducers onto Pt interdigitated electrodes forming an array of sensing units. This e-tongue system was able to detect the phenothiazine methylene blue (MB) below nanomolar concentrations. SERRS was applied to investigate the MB molecular arrangement (monomers or aggregates) when in contact with the phospholipids at trace levels of concentration. The key point was the adsorption of Ag nanoparticles (AgNPs) within the phospholipid LbL films. This approach did not compromise the e-tongue performance and allowed the recording of in situ SERRS spectra for the LbL films after immersion into MB aqueous solutions. The detection of MB through SERRS gave similar results to those reported in the literature but now with an unprecedented sensitivity.

Since the first report in 1985 of an "electronic tongue" system for analyzing liquids with a sensor array,[1] several similar devices have been presented to evaluate samples with complex composition. Various electrical techniques are used in electronic tongues, especially electrochemical methods[2] and *ac* impedance spectroscopy.[3] In the latter approach, the sensing units consist of interdigitated electrodes covered with ultrathin films (in nanometer thickness), whose high sensitivity allows detecting analytes at concentrations down to nanomolar or below. Indeed, these electronic tongues have been used in detecting analytes relevant to the environment,[4−9] in beverage classification,[10−12] in assessing tastants through their functional characteristics,[11,13,14] and in detecting pharmaceutical drugs.[15,16] The films are produced with the Langmuir−Blodgett (LB), layer-by-layer (LbL), and physical vapor deposition (PVD) methods, for which a variety of materials can be used, including conducting polymers, dyes, biomolecules, and organic−inorganic composites leading to the named global selectivity.[17] More recently, the immobilization of enzymes on nanostructured films has been applied in specific sensors that are also highly sensitive.[18−20] The field was developed with new

* Corresponding author. E-mail: case@fct.unesp.br.
† Unesp Univ Estadual Paulista.
‡ University of Valladolid.
§ Universidade Federal de São Carlos.

(1) Otto, M.; Thomas, J. D. R. *Anal. Chem.* **1985**, *57*, 2647–2651.
(2) Ciosek, P.; Wroblewski, W. *Analyst* **2007**, *132*, 963–978.
(3) Riul, A., Jr.; Santos, D. S., Jr.; Wohnrath, K.; Di Tommazo, R.; Carvalho, A. C. P. L. F.; Fonseca, F. J.; Oliveira, O. N., Jr.; Taylor, D. M.; Mattoso, L. H. C. *Langmuir* **2002**, *18*, 239–245.
(4) Olivati, C. A.; Riul, A., Jr.; Balogh, D. T.; Oliveira, O. N., Jr.; Ferreira, M. *Bioprocess Biosyst. Eng.* **2009**, *32*, 41–46.
(5) Volpati, D.; Alessio, P.; Zanfolim, A. A.; Storti, F. C.; Job, A. E.; Ferreira, M.; Riul, A., Jr.; Oliveira, O. N., Jr.; Constantino, C. J. L. *J. Phys. Chem. B* **2008**, *112*, 15275–15282.
(6) Martins, G. G.; Pereira, A. A.; Straccalano, B. A.; Antunes, P. A.; Pasquini, D.; Curvelo, A. A. S.; Ferreira, M.; Riul, A., Jr.; Constantino, C. J. L. *Sens. Actuators, B: Chem.* **2008**, *129*, 525–530.
(7) Carvalho, E. R.; Consolin, N.; Firmino, A.; Oliveira, O. N., Jr.; Mattoso, L. H. C.; Martin-Neto, L. *Sens. Lett.* **2006**, *4*, 129–134.
(8) Carvalho, E. R.; Filho, N. C.; Venancio, E. C.; Oliveira, O. N., Jr.; Mattoso, L. H. C.; Martin-Neto, L. *Sensors* **2007**, *7*, 3258–3271.
(9) Silva, B. A.; Antunes, P. A.; Pasquini, D.; Curvelo, A. A. S.; Aroca, R. F.; Riul, A., Jr.; Constantino, C. J. L. *J. Nanosci. Nanotechnol.* **2007**, *7*, 510–514.
(10) Wu, R. J.; Yeh, C. H.; Yu, M. R.; Chen, H. W. *Sens. Lett.* **2008**, *6*, 765–770.
(11) Constantino, C. J. L.; Antunes, P. A.; Venancio, E. C.; Consolin, N.; Fonseca, F. J.; Mattoso, L. H. C.; Aroca, R. F.; Oliveira, O. N., Jr.; Riul, A., Jr. *Sens. Lett.* **2004**, *2*, 95–101.
(12) Riul, A., Jr.; Sousa, H. C.; Malmegrim, R. R.; Santos, D. S.; Carvalho, A. C. P. L. F.; Fonseca, F. J.; Oliveira, O. N., Jr.; Mattoso, L. H. C. *Sens. Actuators, B: Chem.* **2004**, *98*, 77–82.
(13) Liu, Q. J.; Yu, J. J.; Liu, Z. B.; Zhang, W.; Wang, P.; Yang, M. In *7th Asian-Pacific Conference on Medical and Biological Engineering, Book Series: IFMBE Proceedings*; Peng, Y., Weng, X., Eds.; Springer: New York, 2008;Vol. 19, pp 306−308.
(14) Ferreira, M.; Riul, A., Jr.; Wohnrath, K.; Fonseca, F. J.; Oliveira, O. N., Jr.; Mattoso, L. H. C. *Anal. Chem.* **2003**, *75, 4*, 953–955.
(15) Aoki, P. H. B.; Caetano, W.; Volpati, D.; Riul, A., Jr.; Constantino, C. J. L. *J. Nanosci. Nanotechnol.* **2008**, *8*, 4341–4348.
(16) Tsekenis, G.; Garifallou, G. Z.; Davis, F.; Millner, P. A.; Pinacho, D. G.; Sanchez-Baeza, F.; Marco, M. P.; Gibson, T. D.; Higson, S. P. J. *Anal. Chem.* **2008**, *80*, 9233–9239.
(17) Toko, K. *Meas. Sci. Technol.* **1998**, *9*, 1919–1936.

10.1021/ac902585a
Published on Web 04/02/2010

instrumentation to reach low cost devices,[21,22] application of theoretical[23] and data processing, and computational methods.[12,24]

The high sensitivity and usefulness of the electronic tongues based on impedance spectroscopy have been proven beyond doubt, but a major challenge is to understand why sensitivity is so high. More specifically, one would like to determine the exact nature of the interactions established between the transducer thin films and the analytes at the very low concentrations (nanomolar). It is believed that the chemical composition and the structure of the interface between the thin film and the liquid sample play a key role in reaching high sensitivity.[25−27] However, obtaining structural information at such low level of dilution requires techniques able to combine sensitivity, chemical analysis, and spatial resolution, in addition to being preferably nondestructive. In this context, the surface-enhanced Raman scattering (SERS) or surface-enhanced resonance Raman scattering (SERRS) coupled to optical microscopy (Raman microscopy system) is probably one of the best candidates to comply with these requirements. It might be worth mentioning that SERRS is achieved when the laser line used is in resonance with the UV−vis absorption spectrum of both the metal nanoparticles, which is a necessary condition to achieve SERS, and the target analyte, which is a necessary condition to achieve RRS.

The origin of the SERS effect comes from Fleischmann et al.[28] who in 1974 observed a surprising enhancement of the Raman signal of pyridine on a rough Ag electrode. In 1977, the groups of Jeanmaire and Van Duyne[29] and Albrecht and Creighton[30] solved the puzzle in an independent way. They found that the effect was due to the enhancement of the electromagnetic field of the incoming light by the Ag nanoparticles (AgNPs), whose detailed mechanism is given in ref 31. The improvement of the laser and detector technologies and the understanding of the SERS mechanism itself led to the SERS technique being applied even in detecting single molecules.[32] Various types of enhancers have been used, such as metallic nanoparticles (usually Ag and Au) in different forms such as colloid,[33] large nanoparticles (probably aggregates),[34] and thermally evaporated thin films.[35] In addition to single molecule detection, which is the ultimate limit in terms of chemical analysis, the SERS technique has been applied to characterize a wide range of materials,[36,37] now including biological systems, as in the identification and classification of virus or cancer cells,[38,39] biochemical diagnostics,[40,41] pH sensors,[42] and pharmaceutical drugs.[43]

The SERS enhancement is normally 10^6 on average, but under regime of single molecule detection, it may reach 10^{14} as estimated by Kneipp et al.[33] and Nie et al.[34] or 10^9-10^{11} as reported by Blackie et al.[44] It is known that higher enhancement factors are obtained with aggregates or clusters,[45−47] and different strategies have been developed to produce highly SERS-active substrates.[48−50] Recently, we reported the use of AgNPs trapped within a phospholipid matrix grown in the form of LbL films to achieve the SERRS effect,[51] which can be applied as a proof-of-principle to investigate interactions between guest molecules and phospholipids in membrane mimetic systems. This strategy was based on a previous work where the growth of LbL films containing phospholipids as biological membrane mimetic systems was developed[25] and applied as sensing units through impedance spectroscopy.

Here, impedance spectroscopy and SERRS were combined to achieve high sensitivity, distinguishing ability, and chemical information. Overall, impedance spectroscopy is a powerful, noninvasive, and sensitive technique largely employed to characterize the physical and chemical properties of solid, liquid, and gaseous materials.[52] The sensing units comprised LbL films made with the phospholipids dipalmitoyl phosphatidyl glycerol (DPPG) or cardiolipin (CLP), with and without AgNPs, deposited onto interdigitated electrodes. Impedance spectroscopy measurements were taken with the units immersed into methylene blue (MB)

(18) Caseli, L.; Perinotto, A. C.; Viitala, T.; Zucolotto, V.; Oliveira, O. N., Jr. *Langmuir* **2009**, *25*, 3057–3061.
(19) Moraes, M. L.; Souza, N. C.; Hayasaka, C. O.; Ferreira, M.; Rodrigues, U. P.; Riul, A., Jr.; Zucolotto, V.; Oliveira, O. N., Jr. *Mater. Sci. Eng. C-Biomimetic Supramolecular Syst.* **2009**, *29*, 442–447.
(20) Esseghaier, C.; Bergaoui, Y.; ben Fredj, H.; Tlili, A.; Helali, S.; Ameur, S.; Abdelghani, A. *Sens. Actuators, B: Chem.* **2008**, *134*, 112–116.
(21) Cabral, F. P. A.; Bergamo, B. B.; Dantas, C. A. R.; Riul, A.; Giacometti, J. A. *Rev. Sci. Instrum.* **2009**, *80*, Article Number: 026107.
(22) Pioggia, G.; Di Francesco, F.; Marchetti, A.; Ferro, M.; Ahluwalia, A. *Biosens. Bioelectron.* **2007**, *22*, 2618–2623.
(23) Taylor, D. M.; Macdonald, A. G. *J. Phys. D: Appl. Phys.* **1987**, *20*, 1277–1283.
(24) Jolliffe, I. T. *Principal Compontent Analysis*, Springer-Verlag: Berlin, 2002.
(25) Aoki, P. H. B.; Volpati, D.; Riul, A., Jr.; Caetano, W.; Constantino, C. J. L. *Langmuir* **2009**, *25*, 2331–2338.
(26) Rosei, F. *J. Phys.: Condens. Matter* **2004**, *16*, S1373–S1436.
(27) Silva, H. S.; Miranda, P. B. *J. Phys. Chem. B* **2009**, *113*, 10068–10071.
(28) Fleischmann, M.; Hendra, P. J.; McQuillan, A. J. *Chem. Phys. Lett.* **1974**, *26*, 163–166.
(29) Jeanmaire, D. L.; Van Duyne, R. P. *J. Electroanal. Chem.* **1977**, *84*, 1–20.
(30) Albrecht, M. G.; Creighton, J. A. *J. Am. Chem. Soc.* **1977**, *99*, 5215–5217.
(31) Moskovitz, M. *Rev. Mod. Phys.* **1985**, *57*, 783–826.
(32) Tolaieb, B.; Constantino, C. J. L.; Aroca, R. *Analyst* **2004**, *129*, 337–341.
(33) Kneipp, K.; Wang, Y.; Kneipp, H.; Perelman, L. T.; Itzkan, I. *Phys. Rev. Lett.* **1997**, *78*, 1667–1670.
(34) Nie, S.; Emory, S. R. *Science* **1997**, *275*, 1102–1106.
(35) Constantino, C. J. L.; Antunes, P. A.; Lemma, T.; Aroca, R. *Anal. Chem.* **2001**, *73*, 3674–3678.
(36) Aroca, R. *Surface-Enhanced Vibrational Spectroscopy*; John Wiley & Sons: Toronto, 2006.
(37) Kneipp, K.; Moskovitz, M.; Kneipp, H. *Surface-enhanced Raman Scattering: Physics and Applications*, Springer-Verlag: Duesseldorf, 2006.
(38) Shanmukh, S.; Jones, L.; Zhao, Y. P.; Driskell, J. D.; Tripp, R. A.; Dluhy, R. A. *Anal. Bioanal. Chem.* **2008**, *390*, 1551–1555.
(39) Qian, X.; Peng, X. H.; Ansari, D. O.; Yin-Goen, Q.; Chen, G. Z.; Shin, D. M.; Yang, L.; Young, A. N.; Wang, M. D.; Nie, S. *Nat. Biotechnol.* **2007**, *26*, 83–90.
(40) Kim, J. H.; Kim, J. S.; Choi, H.; Lee, S. M.; Jun, B. H.; Yu, K. N.; Kuk, E.; Kim, Y. K.; Jeong, D. H.; Cho, M. H.; Lee, Y. S. *Anal. Chem.* **2006**, *78*, 6967–6973.
(41) Hering, K.; Cialla, D.; Ackermann, K.; Dörfer, T.; Möller, R.; Schneidewind, H.; Mattheis, R.; Fritzsche, W.; Rösch, P.; Popp, J. *Anal. Bioanal. Chem.* **2008**, *390*, 113–124.
(42) Wang, Z.; Bonoiu, A.; Samoc, M.; Cui, Y.; Prasad, P. N. *Biosens. Bioelectron.* **2008**, *23*, 886–891.
(43) Stevenson, R.; Stokes, R. J.; MacMillan, D.; Armstrong, D.; Faulds, K.; Wadsworth, R.; Kunuthur, S.; Suckling, C. J.; Graham, D. *Analyst* **2009**, *134*, 1561–1564.
(44) Blackie, E. J.; Le Ru, E. C.; Etchegoin, P. G. *J. Am. Chem. Soc.* **2009**, *131*, 14466–14472.
(45) Michaels, A. M.; Normal, M.; Brus, L. E. *J. Am. Chem. Soc.* **1999**, *121*, 9932–9939.
(46) Kneipp, K.; Kneipp, H.; Manoharan, R.; Hanlon, E. B.; Itzkan, I.; Dasari, R. R.; Feld, M. S. *Appl. Spectrosc.* **1998**, *52*, 1493–1497.
(47) Corni, S.; Tomasi, J. *J. Chem. Phys.* **2002**, *116*, 1156–1164.
(48) Oh, N.; Kim, J. H.; Jin, S.; Yoon, C. S. *Small* **2009**, *5*, 1311–1317.
(49) Yang, M. X.; Chen, T.; Lau, W. S.; Wang, Y.; Tang, Q. H.; Yang, Y. H.; Chen, H. Y. *Small* **2009**, *5*, 198–202.
(50) Ko, H.; Singamaneni, S.; Tsukruk, V. V. *Small* **2008**, *4*, 1576–1599.
(51) Aoki, P. H. B.; Alessio, P.; De Saja, J. A.; Constantino, C. J. L. *J. Raman Spectrosc.* **2010**, *41*, 40–48.
(52) MacDonald, J. R. *Impedance Spectroscopy: Emphasizing Solid Materials and Systems*; John Wiley and Sons: New York, 1987.

aqueous solutions down to 10^{-11} M. The SERS spectra were collected directly from the sensing units after their immersion into the MB aqueous solution (in situ SERRS). The growth of the LbL films containing CLP and PAH was monitored using ultraviolet−visible (UV−vis) and Fourier transform infrared (FT-IR) absorption spectroscopies and optical microscopy. MB was chosen due to its therapeutic properties acting as antimicrobial (bacteria, virus, and fungi) compound and as photosensitizer in photoantimicrobial chemotherapy.[53]

EXPERIMENTAL SECTION

Reagents. Anionic phospholipids DPPG (1,2-dipalmitoyl-*sn*-3-glycero-[phosphor-rac-(1-glycerol), purity >99%]) and CLP (1,3-Di (3-*sn*-Fosfatidil)-*sn*-glicerol) were purchased from Avanti Polar Lipids Inc. MB (phenothiazine methylene blue), PAH (poly(allylamine hydrochloride)), sodium citrate ($C_6H_5Na_3O_7 \cdot 2H_2O$ and MW = 294.1 g/mol), and silver nitrate ($AgNO_3$ and MW = 169.88 g/mol) were acquired from Sigma-Aldrich Co. All chemicals were used without further purification. The molecular weights of DPPG, CLP, and MB are 745, 1422, and 319 g/mol, respectively. Ultrapure water (18.2 MΩ.cm and pH 5.6) was obtained from a Milli-Q system, model Simplicity, and used to prepare the solutions and LbL films.

Solutions and Films. The LbL films were fabricated using DPPG, CLP, PAH, and AgNP aqueous solutions. The following concentrations were used: DPPG, 0.74 mg/mL (1.0 mM); CLP, 1.42 mg/mL (1 mM); PAH, 0.80 mg/mL; and MB, 0.32 mg/mL (1.0 mM). The solutions were prepared without any special procedure: the powder was simply added to ultrapure water, and the solution was gently stirred. The Ag colloid was obtained by sodium citrate reduction of silver nitrate following the method proposed by Lee and Meisel[54] and used as synthesized. Briefly, the Ag colloid was prepared by dissolving 90 mg of silver nitrate in 500 mL of ultrapure water, and it was heated until boiling. Then, the solution was stirred, and 10 mL of an aqueous solution of sodium citrate at 1% w/v was added by dropping. The solution was kept boiling under stirring for 1 h. The final concentration of the Ag colloid was ca. 1.0×10^{-3} mol/L.

The PAH/CLP LbL film was fabricated by immersions of the substrate into distinct solutions according to the following sequence: PAH solution (3 min) → ultrapure water gently stirred to remove the excess of adsorbed PAH → CLP (3 min) → ultrapure water to remove excess of adsorbed CLP. Then, the first bilayer PAH/CLP was formed, and the multilayered PAH/CLP LbL film was grown repeating the "four-step sequence". For the growth of multilayered PAH/(CLP+AgNP) LbL films, the same "four-step sequence" was followed. In this case, 2 mL of Ag colloid stock solution were added to a volumetric flask of 10 mL, which was further filled with CLP stock solution. The final concentration of CLP in the (CLP+Ag colloid) aqueous solution was 1.13 mg/mL (0.8 mM). The PAH/DPPG and PAH/(DPPG+AgNP) LbL films were fabricated following the same method whose details are given in Aoki et al.[51] All the LbL films were fabricated using a mechanical dipper available in a Langmuir trough KSV 2000 for lifting and lowering the substrates perpendicularly to the solutions (and washing ultrapure water) at ca. 17 mm/min. This methodology allows fabricating reproducible LbL films.

The number of deposited LbL bilayers and the type of substrate were chosen according to the characterization technique. For instance, the films were grown onto quartz plates for UV−vis absorption spectroscopy and optical microscopy (14 bilayers), onto ZeSe for FT-IR (14 bilayers) and onto interdigitated Pt electrodes for impedance spectroscopy and SERRS (5 bilayers). All substrates were previously cleaned using neutral detergent, being extensively washed with distilled water, acetone (5 min sonication), chloroform (5 min sonication), and ultrapure water. This procedure was sufficient to activate the substrate surfaces for the adsorption of the PAH layer avoiding using any other drastic treatment such as piranha solution (a mixture of concentrated sulphuric acid and hydrogen peroxide).

Characterization Techniques. UV−vis absorption spectroscopy was carried out using a Varian spectrophotometer, model Cary 50, from 190 to 1100 nm. The SEM images were recorded using a FEI microscope, model Quanta 200F, under low vacuum (1.0 Torr) and metalizing the LbL film surfaces (5 nm Au mass thickness). The FT-IR spectra were taken at ambient air using a Bruker spectrometer, model Vector 22, equipped with a DTGS detector. The Raman spectra (RRS and SERRS) and optical microscopy were obtained using a micro-Raman Renishaw spectrograph, model in-Via, equipped with a Leica microscope, whose 50× (NA 0.75) objective lens allows collecting the spectra with ca. 1 μm^2 spatial resolution. The system also contained a CCD detector, laser at 633 nm, 1800 grooves/mm grating with additional notch filters, and a computer-controlled three-axis-encoded (XYZ) motorized stage to take Raman images with a minimum step of 0.1 μm. The spectral collection time used for all SERRS and RRS spectra was 10 s. The SERRS spectra were collected directly from the sensing units used in the impedance experiments.

Impedance spectroscopy (capacitance vs frequency) measurements were carried out with a Solartron 1260A impedance analyzer. The sensor array was composed by five sensing units: a bare Pt electrode and Pt interdigitated electrodes coated with 5-bilayer LbL films of PAH/CLP, PAH/DPPG, PAH/(CLP+AgNP), and PAH/(DPPG+AgNP). The bare Pt electrode was kept as a control to check alterations in the electrical response of the interdigitated electrodes caused by the LbL films. Impedance spectra were acquired in the frequency range 1 Hz to 1 MHz, using 50 mV of amplitude, with the electrodes immersed into ultrapure water (18.2 MΩ·cm), used as reference, and in MB aqueous solutions at 10^{-7}, 10^{-9}, and 10^{-11} M. The electrodes were left soaking for 20 min to enable a stable reading, followed by five consecutive runs at each sensing unit to check variations prior to the data acquisition. Measurements were carried out from the lowest to the highest concentrations, and reference spectra were obtained with ultrapure water. Between each set of measurements, the sensing units were immersed for 10 min in ultrapure water at moderate stirring. It should be mentioned that, before dipping the sensing units into a specific MB solution, they were rinsed with the MB solution to avoid interferences from the presence of trapped water within the films that might alter the concentration of the measured solution and, consequently, the electrical data.

(53) Wainwright, M.; Mohr, H.; Walker, W. H. *J. Photochem. Photobiol., B: Biol.* **2007**, *86*, 45–58.
(54) Lee, P. C.; Meisel, D. *J. Phys. Chem.* **1982**, *86*, 3391–3395.

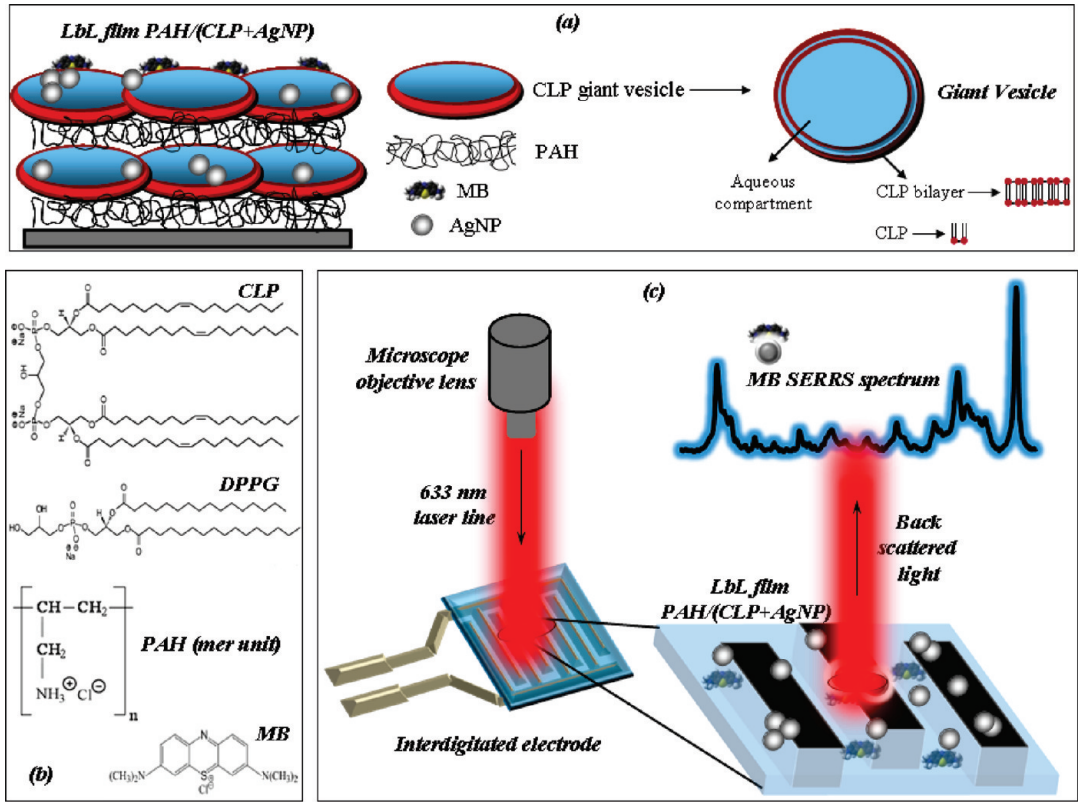

Figure 1. (a) Illustration of the molecular architecture of the LbL films and the CLP giant vesicle. (b) Molecular structure of CLP, DPPG, MB, and PAH mer unit. (c) Illustration of the experimental setup for collecting in situ SERRS spectrum directly from the sensing unit.

Experimental Setup. Figure 1 shows a scheme illustrating the experimental setup and the molecular structures of CLP, DPPG, MB, and PAH mer unit. It is worth noting that, besides the enhancement of the Raman signal achieved by SERRS, the light is scattered by both isolated and aggregated AgNPs, which also improves the signal spatial resolution.

RESULTS AND DISCUSSION

Growth of PAH/CLP and PAH/(CLP+AgNP) LbL films. The growth of LbL films containing PAH, CLP, and AgNPs was systematically monitored by UV−vis absorption spectroscopy. Figure 2a,b shows the UV−vis absorption spectra for the PAH/CLP and PAH/(CLP+AgNP) LbL films, respectively. (See Figure 1a for the schematic structure of the LbL film.) The linear dependence of the absorbance vs number of deposited bilayers (insets) reveals that approximately the same amount of material was adsorbed onto PAH per deposited bilayer, leading to a uniform growth of the LbL films. For PAH/(CLP+AgNP), both CLP and AgNPs compete for the NH_3^+ groups of PAH because CLP is an anionic phospholipid (PO_4^-), and AgNPs are negatively charged.[55] The linear increase in absorbance at ca. 230 nm attributed to CLP and at 430 nm attributed to the AgNP surface plasmon modes[56] indicates that both materials are adsorbed onto PAH. The tail at longer wavelengths in the UV−vis absorption spectrum of PAH/(CLP+AgNP) LbL films is assigned to AgNP aggregates.[56] The electrostatic interactions between NH_3^+ and PO_4^- were identified

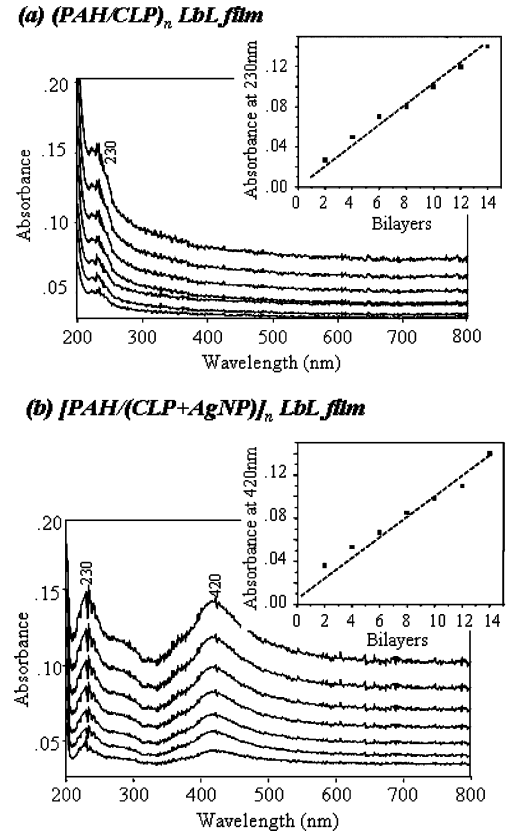

Figure 2. UV−vis absorption spectra for the LbL films of (a) PAH/CLP and (b) PAH/(CLP+AgNP). The insets show the absorbance vs number of deposited bilayers for both LbL films.

(55) Alvarez-Puebla, R. A.; Arceo, E.; Goulet, P. J. G.; Garrido, J. J.; Aroca, R. F. *J. Phys. Chem. B* **2005**, *109*, 3787–3792.
(56) Pieczonka, N. P. W.; Goulet, P. J. G.; Aroca, R. F. *J. Am. Chem. Soc.* **2006**, *128*, 12626–12627.

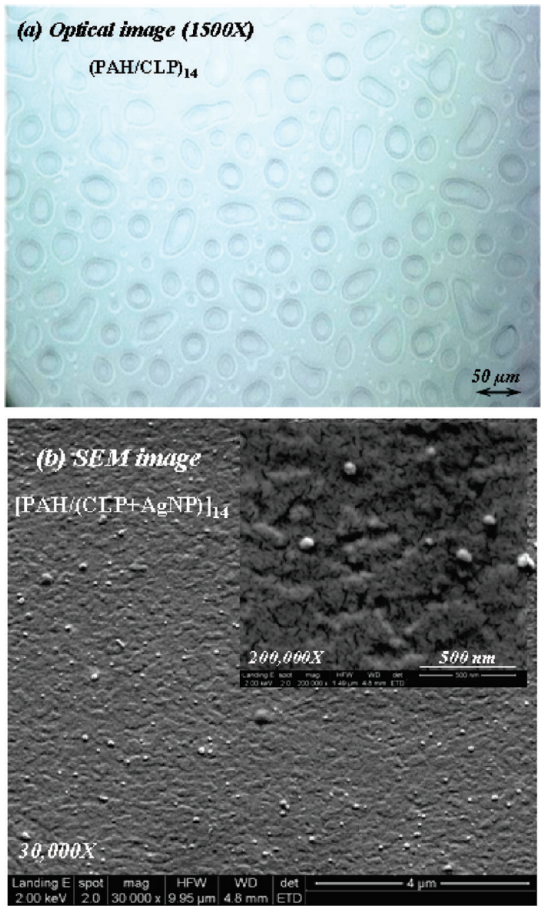

Figure 3. (a) Optical image for the LbL film containing 14 bilayers of PAH/CLP. (b) SEM image for the LbL film containing 14 bilayers of PAH/(CLP+AgNP). The inset shows the AgNPs in detail.

via FT-IR characterization[25] of PAH/DPPG and PAH/DPPC LbL films. Significantly, only a few bilayers could be deposited in the system containing DPPC, for this phospholipid is zwitterionic.

Morphology of PAH/CLP and PAH/(CLP+AgNP) LbL Films. Figure 3a shows the optical image for a 14-bilayer PAH/CLP LbL film deposited onto a quartz plate used in the UV−vis absorption experiments. CLP is seen to form spherical-like vesicles ranging between 4 and 60 μm, with an average size of ~20 μm, characteristic of giant vesicles that are sufficiently large to be seen with optical microscopy. The main techniques used nowadays to prepare giant (phospho)lipid vesicles derive from electroformation[57] and gentle hydration (or natural swelling),[58] where a dried film serves as the starting point. A comparison between both methods was reported by Rodriguez et al.[59] From the contrast shown at the edge of the CLP giant vesicles (Figure 3a) and according to Rodriguez et al.,[59] it can be inferred that these giant vesicles present the so-called "nest of vesicles", which means that the vesicle contains at least another vesicle whose diameter is more than 80% of the larger one.[59] (See Figure 1a for the schematic representation of the CLP giant vesicle.) The CLP giant vesicles might be formed in solution when prepared without any special procedure (hydration or electroformation), with the structure preserved after transfer onto the substrate. Therefore, the methodology applied here could be seen as an alternative to produce giant vesicles of CLP when a sharp distribution of size and shape is not required, which is our case. A few reports exist about CLP giant vesicles, normally formed from a mixture of (phospho)lipids,[60−62] which makes it difficult to compare with our results. Interestingly, using the same procedure described here for LbL films of PAH/DPPG and PAH/DPPC,[25] smaller vesicles were found (0.1−0.3 μm in size), which were characterized as multilamellar vesicles (MLVs, see ref 25 and references therein). In the SEM image for a 14-bilayer PAH/(CLP+AgNP) LbL film in Figure 3b, it is possible to observe the AgNPs dispersed along the surface of the LbL film, which are seen either as isolated or as aggregated particles, supporting the UV−vis absorption spectroscopy results (Figure 2b).

Growth Mechanism to Form PAH/CLP LbL Films. The presence of CLP and PAH in the LbL films was confirmed using FT-IR in the transmission mode. Figure 4 shows the FT-IR spectra for a 14-bilayer PAH/CLP LbL film deposited onto ZnSe and cast films of CLP and PAH (both from aqueous solution). The FT-IR regions below 1900 cm^{-1} and above 2750 cm^{-1} are given in the zooms, featuring absorption bands of both CLP and PAH in the LbL film. Table 1 brings the assignments of the main FT-IR bands for both CLP[63,64] and PAH[65,66] cast films. Since the main bands of CLP and PAH appeared in the cast films, the interactions between CLP and PAH can be inferred following changes in the PAH/CLP LbL film. For instance, the band at 1235 cm^{-1} (PO_2^- antisymmetric) for the CLP cast film shifted to 1215 cm^{-1} in the LbL film, and the band at 1098 cm^{-1} (PO_2^- symmetric) had its relative intensity altered in relation to the adjacent bands at 1067 and at 1035 cm^{-1}. Besides, the bands at 838 and 886 cm^{-1} (P−O stretching) for the CLP cast film coalesced into a broader band with maximum at 840 cm^{-1} for the PAH/CLP LbL film. As for PAH, the bands at 1514 and 1613 cm^{-1} (NH_3^+ bending vibrations) for the cast film shifted to 1536 and 1638 cm^{-1} in the PAH/CLP LbL films. These findings point to the electrostatic interaction between the NH_3^+ groups of PAH and PO_4^- groups of CLP as the main driving force for the adsorption of the LbL films. Similar results were observed for PAH/DPPC and PAH/DPPG LbL films[25] and LB films containing DPPG+PAH.[67] (The PAH was dissolved into the water subphase.) Hubner et al.[63] reported intramolecular hydrogen bonding between phosphate groups and NH_4^+ counterion (ammonium salt of CLP) instead of Na^+ (sodium salt of CLP). This is consistent with the hypothesis of a key role played by the phospholipid polar head groups on the growth of LbL films containing CLP and PAH.

For DPPG, a neat cast film, or for (DPPG+PAH), a LB film,[67] the antisymmetric and symmetric CH_2 stretchings were observed

(57) Angelova, M.; Dimitrov, D. S. *Faraday Discuss. Chem. Soc.* **1986**, *81*, 303–308.
(58) Reeves, J. P.; Dowben, R. M. *J. Cell. Physiol.* **1969**, *73*, 49–60.
(59) Rodriguez, N.; Pincet, F.; Cribier, S. *Colloids Surf., B* **2005**, *42*, 125–130.
(60) Akashi, K.; Miyata, H.; Itoh, H.; Kinosita, K. *Biophys. J.* **1996**, *71*, 3242–3250.
(61) Tomsie, N.; Babnik, B.; Lombardo, D.; Mavcic, B.; Kanduser, M.; Iglic, A.; Kralj-Iglic, V. *J. Chem. Inf. Model.* **2005**, *45*, 1676–1679.
(62) Urbanija, J.; Babnik, B.; Frank, M.; Tomsic, N.; Rozman, B.; Kralj-; Iglic, V.; Iglic, A. *Eur. Biophys. J. Biophys. Lett.* **2008**, *37*, 1085–1095.
(63) Hubner, W.; Mantsch, H. H.; Kates, M. *Biochim. Biophys. Acta* **1991**, *1066*, 166–174.
(64) Casal, H. L.; Mantsch, H. H. *Biochim. Biophys. Acta* **1984**, *779*, 381–401.
(65) Harris, J. J.; Bruening, M. L. *Langmuir* **2000**, *16*, 2006–2013.
(66) Bonazzola, C.; Calvo, E. J.; Nart, F. C. *Langmuir* **2003**, *19*, 5279–5286.
(67) Aoki, P. H. B.; Alessio, P.; Rodrıguez-Mendez, M. L.; De Saja Saez, J. A.; Constantino, C. J. L. *Langmuir* **2009**, *25*, 13062–13070.

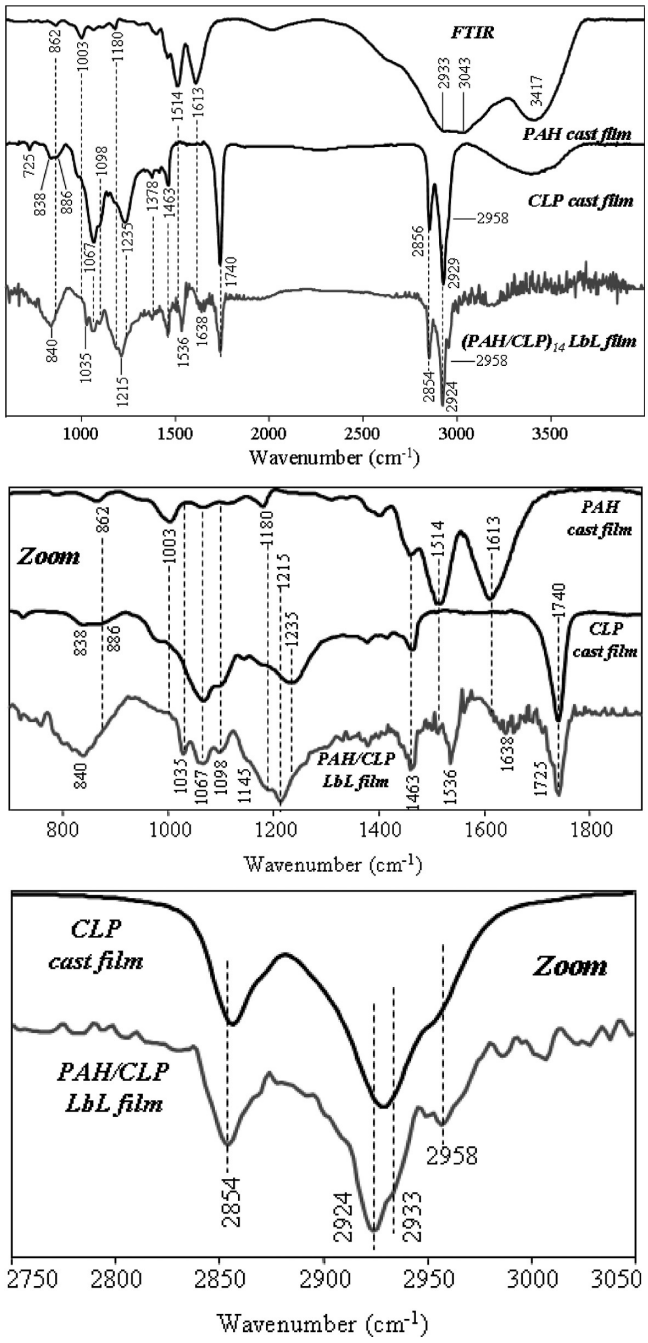

Figure 4. FT-IR spectra recorded for PAH and CLP cast films and PAH/CLP LbL film containing 14 bilayers. The zooms show details of the FT-IR spectra at higher and lower wavenumbers.

at 2917 and 2850 cm^{-1}, respectively, i.e., at lower wavenumbers than for CLP (cast and LbL films, Figure 4). The CH_2 modes are very sensitive to the order, and the latter results indicate that the acyl chains of DPPG are found as bilayers with a high degree of order (solid-like phase); while in the case of CLP, the acyl chains are less ordered (liquid crystalline-like phase).[68,63] Specifically for CLP, it could be inferred that the acyl chain degree of order tends to increase from cast to LbL films (Figure 4), possibly as a consequence of the CLP−PAH interaction.

Sensor Application through Impedance Spectroscopy. The sensing units formed by Pt interdigitated electrodes covered with

(68) Mantsch, H. H. *J. Mol. Struct.* **1984**, *113*, 201–212.

Table 1. Assignments of the Main FT-IR Bands for the CLP and PAH Cast Films

CLP (cm^{-1})	PAH (cm^{-1})	assignments
	3417	N−H stretching[65,66]
	2958	C−H stretching[65,66]
2958 shoulder		CH_3 antisymmetric stretching[63,64]
2929		CH_2 antisymmetric stretching[63,64]
2856		CH_2 symmetric stretching[63,64]
1740		Carbonyl group stretching[63,64]
	1613	NH_3^+ antisymmetric bending vibration[65,66]
	1514	NH_3^+ symmetric bending vibration[65,66]
1463		CH_2 scissoring[63] or antisymmetric deformation modes of the methyl group (umbrella-type)[64]
1378		symmetric deformation modes of the methyl group (umbrella-type)[64]
[a]1235		P═O antisymmetric stretching (PO_2^-group)[63,64]
[a]1098		P═O symmetric stretching (PO_2^- group)[63,64]
1067		C−O−P−O−C vibration[63] or C−O stretching (ester group) coupled to C−C stretchings[64]
886		P−O stretching[64]
838		P−O stretching[64]
725		CH_2 rocking[64]

[a] These modes overlap with the CH wagging band progression, which is a sequence of sharp bands, leading to shoulders or weak bands that appear between 1000 and 1300 cm^{-1}.[64]

the following LbL films: $(PAH/CLP)_5$, $(PAH/DPPG)_5$, $[PAH/(CLP+AgNP)]_5$, and $[PAH/(DPPG+AgNP)]_5$ were immersed into MB aqueous solutions at very low concentrations (10^{-7}, 10^{-9}, and 10^{-11} M). Curves of capacitance vs frequency of the applied voltage were recorded for each MB aqueous solution as shown in Figure 5. The observed trends can be explained by an equivalent electric circuit model.[23] Briefly, in this equivalent circuit model, whose scheme is shown in the inset in Figure 5, the following elements are considered: geometric capacitance of the electrodes (Cg), double layer effects at the electrode/electrolyte interface (Cd and Rd), charge transfer processes (Rt), and the film covering the electrodes (represented by Cb and Rb). The double layer effects are dominant at low frequencies (<50 Hz); the electrode/electrolyte response dominates at an intermediate region, and the geometric capacitance prevails at higher frequencies.[23] The presence of AgNPs trapped in the LbL films strongly alters the electrical response of the electrodes immersed in MB solutions.

It is remarkable that the capacitances tend to increase with increasing MB concentration; while for the films without AgNPs, the trend was opposite, which may be explained as follows: (i) in the absence of AgNPs, MB are physisorbed via electrostatic interactions of the polar head groups of the vesicles on the top layer of DPPG or CLP LbL films. This decreases the number of available PO_4^- sites, causing a decrease in the amount of unbalanced charge at the electrode/electrolyte interface, thus decreasing the capacitance; (ii) with AgNPs within the DPPG or the CLP layer in the LbL films, the MB physisorbed on the top layer again decrease the available PO_4^- sites, but now some of the charged AgNPs inside the LbL film are left unbalanced. Because the nanoparticles are distributed within the film, the increase in capacitance overcompensates the decrease caused by the unavailability of PO_4^- sites, and the capacitance increased with increasing MB concentration, as observed in Figure 5. It must be clarified that the electrostatic interactions between MB, as a

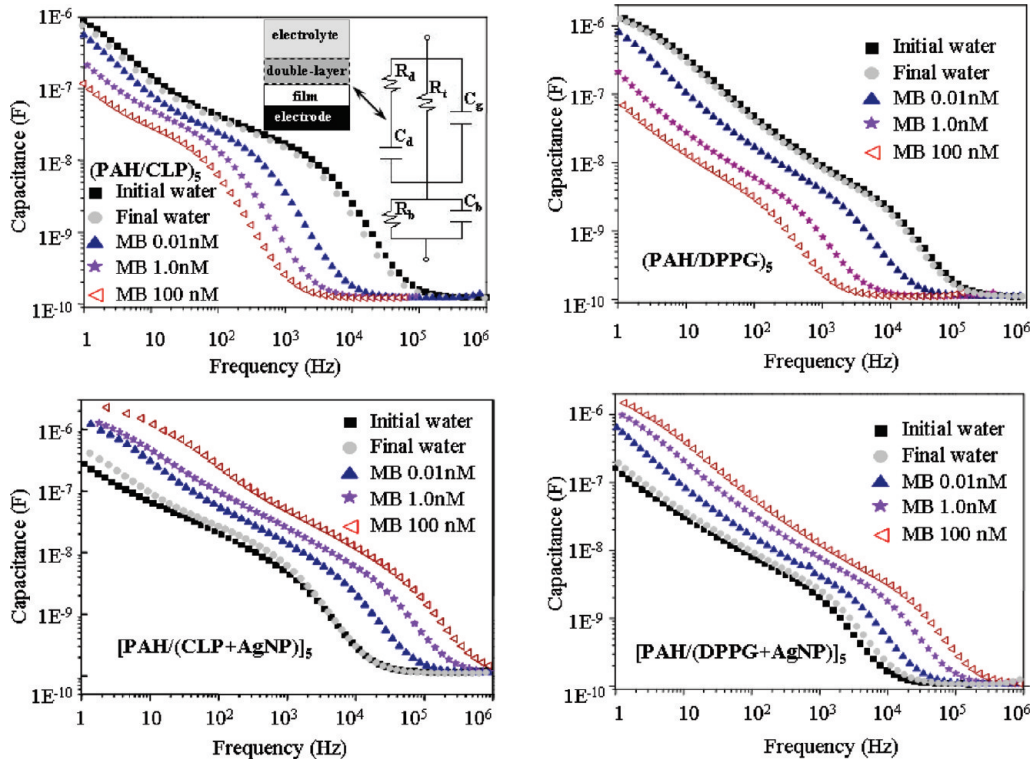

Figure 5. Capacitance vs frequency for the LbL films containing five bilayers deposited onto interdigitated electrodes and immersed into MB aqueous solutions and into ultrapure water before and after the sensing experiments. The inset shows an equivalent electric circuit for modeling the system electrode/film/double layer/electrolyte, where C_g is the geometric capacitance of the electrode, C_d and R_d are related to the double layer effects at the electrode/electrolyte interface, R_t represents the charge transfer processes, and C_b and R_b represent the film covering the electrode.

cationic drug, and DPPG[15,25,67] or CLP,[69] as negatively charged phospholipids, can also happen between MB and AgNPs, which are negatively charged.[51] However, it must be stressed that we refer to the top layers of the LbL films since the MB is adsorbed mainly at the film/electrolyte interface.

The distinct electrical response in Figure 5 suggested that the samples with different MB concentrations could be distinguished, which was confirmed with the PCA plot in Figure 6a. In this plot, data from the bare electrode and the four LbL films were combined, enabling detection of highly diluted MB solutions. Furthermore, a clear trend in the placement of the data points is observed with increasing concentration, with good correlation between the principal components and the MB concentration. In addition, the incorporation of AgNPs in the LbL film structure is clearly noticed in the loading plots in Figure 6b, indicating their strong contribution to PC1, where the highest correlation between samples is established. This can also be illustrated with the changes observed in the electrical response of Figure 5, due to the strong interference brought by the AgNPs at the film interface. A detailed description of the process might not be a simple task due to a collective behavior governed by weak, nonbonding interactions at the molecular level. As shown in the next section, SERRS data revealed that MB adsorbs in the LbL films and its interaction with the surrounding medium changes from spot to spot leading to different patter of spectra.

SERRS Applied to LbL Films. The sensing units used in the impedance spectroscopy measurements were investigated using micro-Raman technique, which combines morphological and chemical information by coupling an optical microscope to a Raman spectrograph. (See the experimental scheme in Figure 1.) Figure 7 shows the optical image for a micrometer domain of MB at the surface of the PAH/(CLP+AgNP) LbL film and several MB SERRS spectra collected from this domain. Figure 8 presents the optical image for another region of the same sensing unit, which does not present the micrometer MB domain at the surface of the LbL film, and several MB SERRS spectra collected from this region (without MB domain). Superposed to the optical images of the sensing units in Figures 7 and 8 are Raman mappings recorded for an area of 60 μm × 60 μm and step of 2 μm leading to a total of 961 spectra. The area mappings were built plotting the intensity of the band at 1623 and 1627 cm^{-1}, respectively, where brighter spots refer to more intense Raman bands. The bands at ca. 1623 and 1393 cm^{-1} are attributed to C=C + C−N=C stretchings, at 1500 and 1302 cm^{-1} are assigned to CC ring stretching, and at 1156 cm^{-1} is assigned to CH bending.[70] It must be said that the Pt fingers in the optical image in Figure 8 appears brighter than those shown in Figure 7 because in Figure 7 the laser was focused onto the MB domains and in Figure 8 the laser was focused directly onto Pt fingers. Therefore, the laser focus is more distant from the Pt fingers in Figure 7 than in Figure 8. This difference in the laser focus generates the difference in the background of each optical image.

From the data in Figures 7 and 8, the main pieces of information extracted are the following: (i) The area Raman mappings are related to the MB SERRS spectra since CLP (or

(69) Hidalgo, A. A.; Caetano, W.; Tabak, M.; Oliveira, O. N., Jr. *Biophys. Chem.* **2004**, *109*, 85–104.

(70) Nicolai, S. H. A.; Rubim, J. C. *Langmuir* **2003**, *19*, 4291–4294.

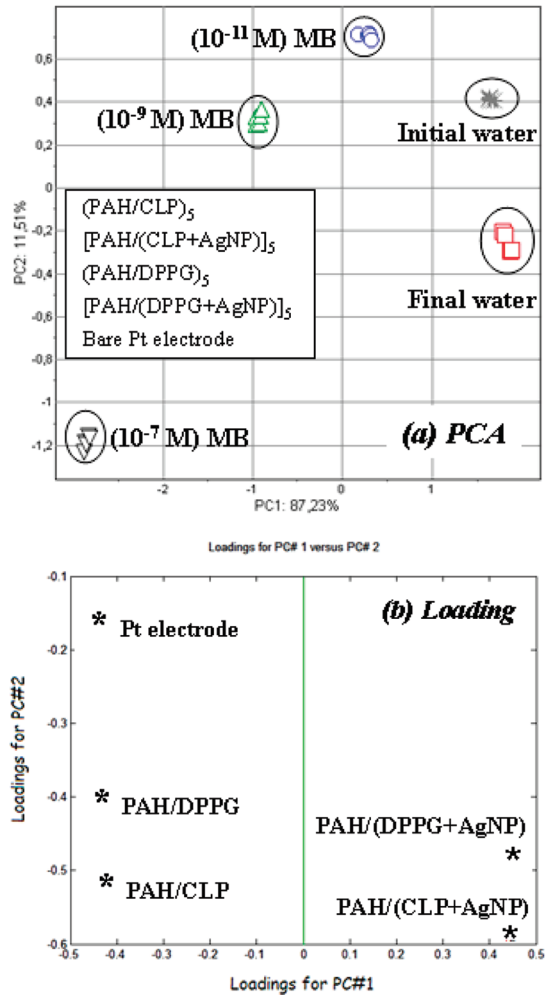

Figure 6. (a) PCA plot built using the capacitance values recorded at 1 kHz for the experiment described in Figure 5. (b) Loadings for PC1 vs PC2.

DPPG) and PAH do not exhibit SERS signal. Besides, Figure 7 shows a RRS spectrum for a MB cast film whose profile is similar to the SERRS recorded for the LbL film in the sensing units. It might be worth mentioning that the MB Raman spectra recorded are named SERRS because the 633 nm laser line used is in resonance with the UV−vis absorption spectrum of both AgNPs (Figure 2b), which is a necessary condition to achieve the surface-enhanced phenomenon, and MB (see the inset in Figure 9), which is a necessary condition to achieve RRS; (ii) The SERRS intensity for the MB micrometer domain in Figure 7 follows the domain spatial distribution according to the optical image, i.e., the SERRS signal is stronger where the MB domain is seen in the optical image. Indeed, since these spectra are from domains of MB, which are not necessarily in contact with AgNPs, one could speculate that they are RRS spectra (instead SERRS); (iii) On the other hand, in the region with no domains at micrometer scale (Figure 8), the MB spectra do refer to SERRS and must follow the AgNPs spatial distribution (Figure 3b). The later is based on the fact that RRS spectra were not observed for regions without MB domains in the sensing units without AgNPs. Besides, considering that the SERS phenomenon is strongly distance dependent regarding the separation between the target molecule and the metal NPs,[31,71,72] the MB must be close enough to the AgNPs to have achieved its SERRS spectrum; (iv) Slight differences in terms of the wave-numbers at higher vibrational frequencies exist between the SERRS spectra from the regions with and without MB micrometer domains. This arises from the level of aggregation of MB in these regions. The latter can be inferred from the relative band intensities between 450 and 500 cm^{-1}. The distinction between MB monomers and aggregates (dimers, trimers, or higher orders of aggregates) is made mainly based on the relative intensity of the band at ca. 480 cm^{-1}, which grows for the monomers when compared to the bands at ca. 450 and 500 cm^{-1}.[73] Therefore, the region with domains contains mainly MB aggregates while the region without domains is dominated by MB monomers. However, it must be stressed that the differences found for the MB SERRS spectra are not worthless; especially for the region without MB domains (more "diluted" MB within the phospholipid matrix). They reveal how susceptible the MB molecule is in relation to its surrounding. We have observed such SERRS spectral variation when working with highly diluted systems toward single molecule detection.[35,74,75] The latter suggests that, despite that MB has two distinct SERRS spectra related to inelastic scattering of the light from MB monomers and aggregates, when reaching a highly diluted system, approaching to single molecule conditions, the SERRS spectra can vary significantly depending on MB surrounding. For instance, it is worth mentioning that, in the 10^{-11} M concentration of MB, the number of MB molecules per picoliter (10^{-12} L) is estimated to be 6. The picoliter scale is chosen because this is the order of magnitude of the laser probed volume in single molecule experiments:[76] 30 pL by Kneipp et al.,[33] 2.5 pL by Delfino et al.,[77] 0.152 pL by Blackie et al.,[44] and 0.0314 pL by Zhang et al.[78] For instance, we have reported 1 pL in a previous work[32] for 514.5 nm (50× and NA 0.80 oil immersion microscopic objective) for running the single molecule experiments to detect a perylene derivative in Ag and Au colloids; (v) As previously mentioned (item iii), RRS signal was not detected for regions without MB domains for the LbL films without AgNPs, evidencing the role played by the surface-enhanced phenomenon. Furthermore, immersing the LbL films into aqueous solutions containing MB even at higher concentrations than those used for impedance spectroscopy, no difference was observed either in the FT-IR or in the UV−vis absorption spectra. A rough estimation of the enhancement factor can be made considering the ratio SERRS/RRS for any band of the spectra. For instance, in Figure 9 the ratio for the band at 1627 cm^{-1} is 105 640 counts/5200 counts. Considering that the SERRS was collected with 1% of the laser power and the RRS was collected with 100% of this power, the enhancement factor can be estimated as (105 640 counts/5200 counts) × (100%/1%). The latter leads to an enhancement factor of ca. $2 \times 10,^3$ which is about 1 order of magnitude below the

(71) Kovacs, G. J.; Loutfy, R. O.; Vincett, P. S.; Jennings, C.; Aroca, R. F. *Langmuir* **1986**, *2*, 689–694.
(72) Constantino, C. J. L.; Duff, J.; Aroca, R. *Spectrochim. Acta, Part A* **2001**, *57*, 1249–1259.
(73) Nicolai, S. H. A.; Rodrigues, P. R. P.; Agostinho, S. M. L.; Rubim, J. C. *J. Electroanal. Chem.* **2002**, *527*, 103–111.
(74) Constantino, C. J. L.; Lemma, T.; Antunes, P. A.; Aroca, R. *Spectrochim. Acta, Part A* **2002**, *58*, 403–409.
(75) Constantino, C. J. L.; Lemma, T.; Antunes, P. A.; Goulet, P.; Aroca, R. *Appl. Spectrosc.* **2003**, *57*, 649–654.
(76) Pieczonka, N. P. W.; Aroca, R. F. *Chem. Soc. Rev.* **2008**, *37*, 946–954.
(77) Delfino, I.; Bizzarri, A. R.; Cannistraro, S. *Biophys. Chem.* **2005**, *113*, 41–51.
(78) Zhang, Z. L.; Yin, Y. F.; Jiang, J. W.; Mo, Y. J. *J. Mol. Struct.* **2009**, *920*, 297–300.

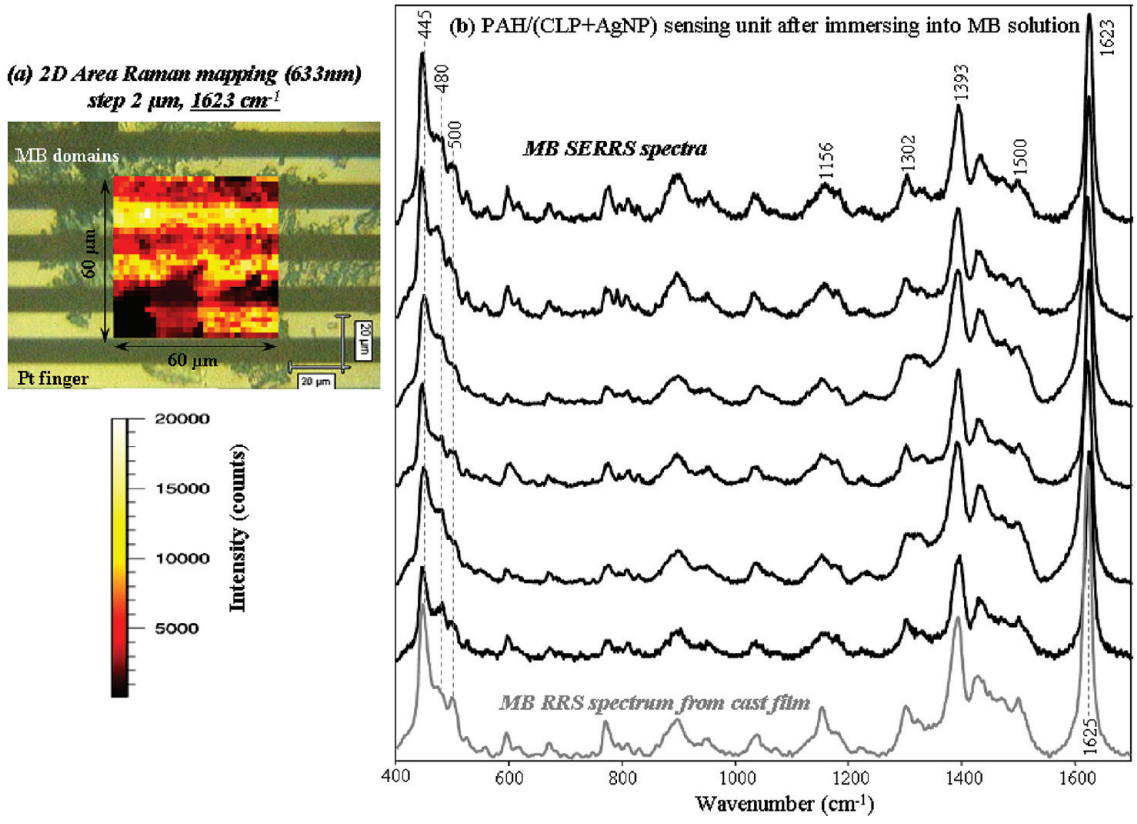

Figure 7. (a) Optical image and Raman mapping (superposed) recorded for the sensing unit $[PAH/(CLP+AgNP)]_5$ after the sensing experiment for an area containing micrometer domains of MB. (b) Several SERRS spectra collected in the mapped area shown in (a). At the bottom is given a RRS spectrum collected for a MB cast film.

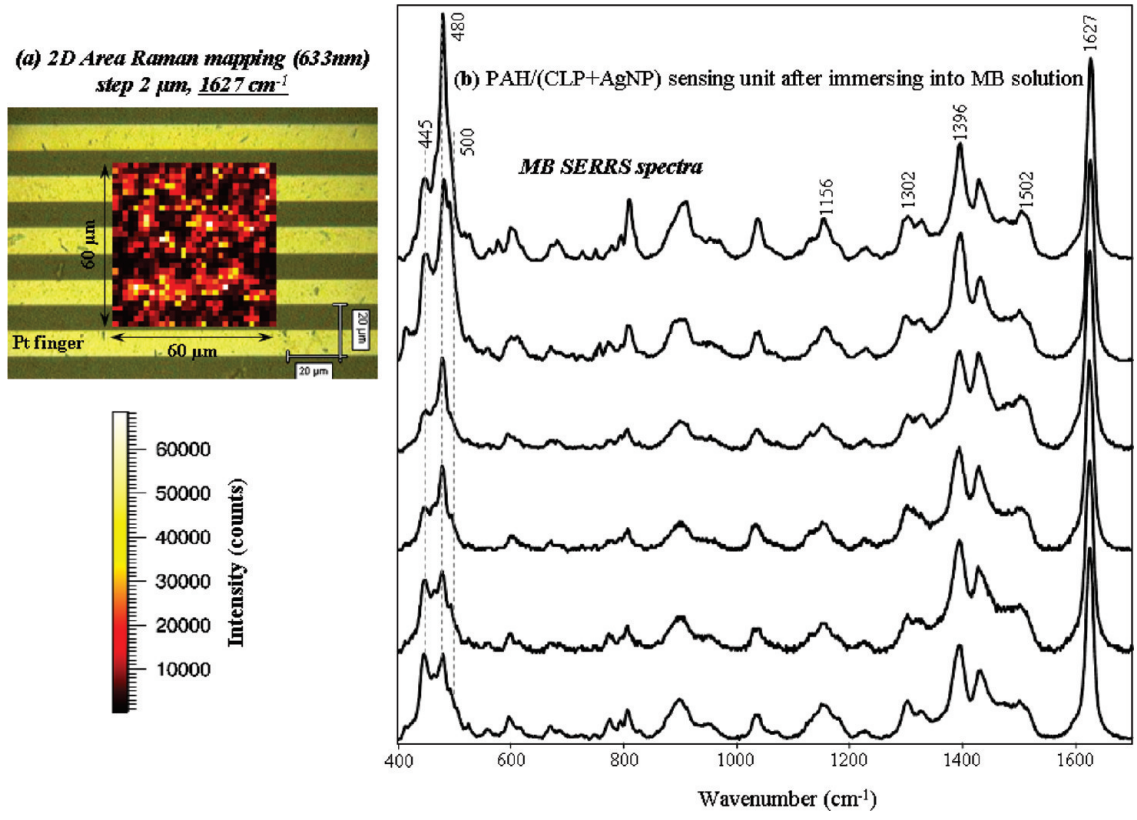

Figure 8. (a) Optical image and Raman mapping (superposed) recorded for the sensing unit $[PAH/(CLP+AgNP)]_5$ after the sensing experiment for an area without micrometer domains of MB. (b) Several SERRS spectra collected in the mapped area shown in (a).

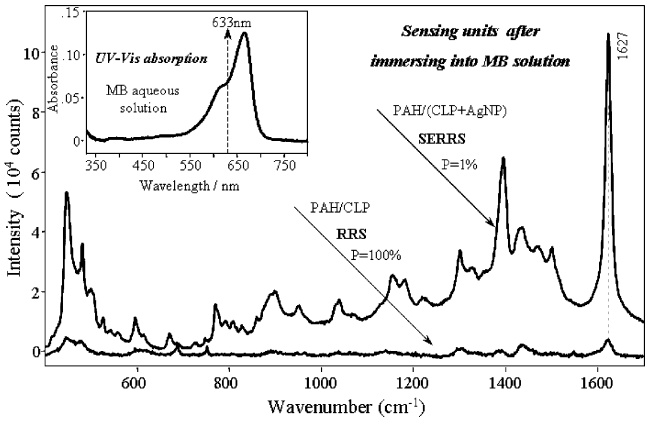

Figure 9. SERRS and RRS spectra recorded for the sensing units with and without AgNPs trapped in the LbL films $(PAH/CLP)_5$ and $[PAH/(CLP+AgNP)]_5$, respectively. The spectra were collected with different laser powers (P), as indicated, and the RRS refers to a spot containing MB domains while the SERRS refers to a spot without these domains (micrometers in size). The inset shows the UV−vis absorption spectrum of the MB aqueous solution (5 μM) and the array at 633 nm laser line used in the Raman experiments.

value reported in our previous work for LbL films of PAH/(DPPG+MB) containing trapped AgNPs.[51] However, it is still in good agreement with the enhancement factors predicted using the electromagnetic mechanism.[79] Besides, it must be mentioned that the concentration of the MB molecules was not considered in this estimation. In fact, the RRS spectrum in Figure 9 was obtained from a MB domain; otherwise, the RRS is not detectable as previously mentioned (items iii and v), while the SERRS spectrum was obtained for a region without MB domain visible at micrometer scale. The latter plays in favor of increasing the intensity of the RRS, which leads to a decrease of the estimated enhancement factor considering the ratio SERRS/RRS.

(79) Tarcha, P. J.; De Saja-Gonzalez, J.; Rodriguez-Llorente, S.; Aroca, R. F. *Appl. Spectrosc.* **1999**, *53*, 43–48.

CONCLUSIONS

PAH/CLP LbL films with and without AgNPs trapped within the phospholipid matrix were successfully grown. As expected, the electrostatic interaction between the groups of NH_3^+ of PAH and PO_4^- of CLP was the main driving force for adsorption of PAH/CLP LbL films. In terms of morphology, CLP forms giant vesicles (micrometers in average) with a relatively wide distribution of size and shape. The LbL films grown from the solution containing phospholipid and Ag colloid present the AgNPs dispersed along the film as either isolated or aggregated particles. The PAH/CLP and PAH/(CLP+AgNP) LbL films were deposited onto Pt interdigitated electrodes forming sensing units, which were applied in the detection of methylene blue (MB) down to 10^{-11} M concentrations. The Raman analysis of the sensing units after immersion into MB solutions revealed that the AgNPs present in the LbL films achieves the MB SERRS spectra allowing not only the detection at this level of dilution but also the distinction of the molecular arrangement assumed by MB (monomers or aggregates, mainly). Besides, due to the high dilution of this system (10^{-11} M), the MB SERRS spectra recorded for the regions of the LbL film dominated by MB monomers presented significant variations from spot to spot of the film. The latter is similar to what is found when approaching single molecule detection for other dyes.

ACKNOWLEDGMENT

FAPESP, CNPq, and CAPES (process 118/06) from Brazil and MICINN (PHB2005-0057-PC) from Spain are acknowledged for the financial support.

Received for review November 11, 2009. Accepted March 22, 2010.

AC902585A